



THE UNIVERSITY *of* EDINBURGH

Edinburgh Research Explorer

Semi-empirical correlations for predicting hot gas layer temperature in pre-flashover compartment fires considering fire source location

Citation for published version:

Lemmertz, CK, Helfenstein, RP, Beshir, M, Rush, D, Jahn Von Arnswaldt, W & Roman Centeno, F 2022, 'Semi-empirical correlations for predicting hot gas layer temperature in pre-flashover compartment fires considering fire source location', *Journal of the Brazilian Society of Mechanical Sciences and Engineering*, vol. 44, 195. <https://doi.org/10.1007/s40430-022-03431-z>

Digital Object Identifier (DOI):

[10.1007/s40430-022-03431-z](https://doi.org/10.1007/s40430-022-03431-z)

Link:

[Link to publication record in Edinburgh Research Explorer](#)

Document Version:

Peer reviewed version

Published In:

Journal of the Brazilian Society of Mechanical Sciences and Engineering

General rights

Copyright for the publications made accessible via the Edinburgh Research Explorer is retained by the author(s) and / or other copyright owners and it is a condition of accessing these publications that users recognise and abide by the legal requirements associated with these rights.

Take down policy

The University of Edinburgh has made every reasonable effort to ensure that Edinburgh Research Explorer content complies with UK legislation. If you believe that the public display of this file breaches copyright please contact openaccess@ed.ac.uk providing details, and we will remove access to the work immediately and investigate your claim.



[Click here to view linked References](#)

Semi-empirical correlations for predicting hot gas layer temperature in pre-flashover compartment fires considering fire source location

Calisa Katuscia Lemmert^{a,*}, Rodolfo Prediger Helfenstein^a, Mohamed Beshir^b, David Rush^{b,*}, Wolfram Jahn Von Arnswaldt^c, Felipe Roman Centeno^{a,*}

^a *Department of Mechanical Engineering, Federal University of Rio Grande do Sul, Sarmiento Leite Street, 425, Porto Alegre, 90050-170, RS, Brazil.*

^b *School of Engineering, University of Edinburgh, UK*

^c *Department of Mechanical and Metallurgical Engineering, Pontifical Catholic University of Chile, Santiago, Chile*

*Corresponding authors: calisa.lemmertz@ufrgs.br, d.rush@ed.ac.uk, frcenteno@mecanica.ufrgs.br

Abstract. A series of numerical experiments have been carried out through a CFD code namely Fire Dynamics Simulator (FDS) to analyze the influence of the fire heat source location (transversal, longitudinal and vertical positions) on the hot gas layer temperature (HGLT) in pre-flashover compartment fires. Knowing the HGLT helps engineers to predict the onset of flashover and to design fire safety systems, which give more time for evacuation procedures. Using these numerical data, and based on an energy balance on the upper layer, new semi-empirical correlations were developed to predict the HGLT in pre-flashover compartment fires, as a function of the fire source location, heat release rate, ventilation factor, surface area, effective heat transfer coefficient and ambient thermal properties. As an external validation of the newly developed correlations, their outcomes were tested against several sets of experimental data available in the literature, showing a good agreement. So, it is concluded that these improved correlations are capable to predict the HGLT for different pre-flashover fire scenarios, accounting to the position where the fire started.

Keywords: pre-flashover fires; compartment fires; heat source location; hot gas layer temperature; FDS.

Nomenclature

A_o	Opening area [m ²]
$A_o\sqrt{H_o}$	Ventilation factor [m ^{5/2}]
A_T	Total area of the compartment surface [m ²]
c	Wall specific heat [kJ kg ⁻¹ K ⁻¹]
C_p	Specific heat of air [kJ kg ⁻¹ K ⁻¹]
C_V	Deardorff's model constant
D^*	Characteristic fire diameter [m]
f_b'''	Drag force per unit volume [kg m ⁻² s ⁻²]
g	Gravity acceleration [m s ⁻²]
\mathbf{g}	Gravity vector [m s ⁻²]
h	Sensible enthalpy [kJ kg ⁻¹]
\dot{h}_b'''	Fuel enthalpy source term [kW m ⁻³]
h_k	Effective heat transfer coefficient, [kW m ⁻² K ⁻¹]
H	Compartment height [m]

1	H_o	Opening height [m]
2	J_i	Diffusive mass flux of species i [kg m ⁻² s]
3	k	Wall thermal conductivity [kW m ⁻¹ K ⁻¹]
4	k_{sgs}	Subgrid kinetic energy [m ² s ⁻²]
5	$M(x)$	Measure of Turbulence Resolution (MTR)
6	\dot{m}_b'''	Mass source term [kg s ⁻¹ m ⁻³]
7	$\dot{m}_{b,i}'''$	Mass production rate per unit volume of species i by evaporating droplets/particles [kg m ⁻³ s ⁻¹]
8	\dot{m}_i'''	Mass production rate per unit volume of species i by chemical reactions [kg m ⁻³ s ⁻¹]
9	p	Pressure [Pa]
10	p_0	Thermodynamic pressure [Pa]
11	$\dot{q}_{c,b}'''$	Convective heat transfer source term of the fuel [kW m ⁻³]
12	\mathbf{q}	Heat flux vector [kW m ⁻²]
13	\mathbf{q}_r	Radiative heat flux vector [kW m ⁻²]
14	\dot{Q}	Heat release rate [kW]
15	R	Universal gas constant [J mol ⁻¹ K ⁻¹]
16	t	Time [s]
17	t	Exposure time [s]
18	tp	Thermal penetration time [s]
19	T	Temperature [K]
20	TKE	Turbulent kinetic energy per unit mass [m ² s ⁻²]
21	T_L	Lower layer temperature [K]
22	T_U	Upper layer temperature or hot gas layer temperature [K]
23	T_∞	Ambient temperature [K]
24	\mathbf{u}	Velocity vector [m s ⁻¹]
25	u^+	Nondimensional streamwise velocity
26	u_τ	Friction velocity [m s ⁻¹]
27	$\tilde{u}, \tilde{v}, \tilde{w}$	Resolved LES velocity components
28	\bar{W}	molecular weight of the gas mixture [kg mol ⁻¹]
29	y	Distance to the wall [m]
30	Y_i	Mass fraction of species i
31	y^+	Nondimensional wall-normal distance
32	z	Height of the fire source [m]
33	z^*	Dimensionless height

Greek letters

34	α	Correlation first term exponent
35	α_w	Wall thermal diffusivity [m ² s ⁻¹]
36	β	Correlation second term exponent
37	γ	Correlation constant
38	δ	Correlation correction term
39	δ_w	Wall thickness [m]
40	δ_x	Dimensions of the mesh cell [m]
41	δ_v	Viscous length scale [m]
42	Δ	Width filter [m]
43	ΔT	Upper layer temperature rise [K]

61
62
63
64
65

1	κ	Von Kármán constant
2		
3	μ	Dynamic viscosity [Pa s]
4	μ_t	Subgrid-scale turbulent viscosity [Pa s]
5	ν	Kinematic viscosity [$\text{m}^2 \text{s}^{-1}$]
6		
7	ρ	Density [kg m^{-3}]
8	ρ	Wall density [kg m^{-3}]
9		
10	ρ_∞	Ambient air density [kg m^{-3}]
11	τ	Viscous stress tensor [Pa]
12	τ_w	Viscous stress at the wall [Pa]

Superscript

sgs Subgrid scale

Special Operators

$\bar{\phi}(\mathbf{x}, t)$ Conventional implicit spatial filter

$\tilde{\phi}(\mathbf{x}, t)$ Implicit Favre-filter

$\langle \phi(\mathbf{x}, t) \rangle_{vb}$ Explicit anisotropic box filter

$\tilde{D}\phi/\tilde{D}t$ Favre-filtered material derivative

1 Introduction

To adequately design and manage fire safety systems, it is necessary to properly understand fire dynamics and the conditions resulting from a compartment fire. In a pre-flashover compartment fire, hazardous gases and heat are accumulated in the upper portion of the room, which is then denominated as hot gas layer (HGL) or upper layer, and its composition influences on visibility and hazards for occupants.

The hot gas layer temperature (HGLT) in pre-flashover compartment fires is related to several safety issues, such as, the occurrence of hazardous conditions for people, the fire spread to combustible items far from the fire source and the occurrence of flashover (when the entire room is involved in the fire) [1]. Knowing the HGLT in a certain fire scenario helps engineers to predict the onset of flashover and to design fire safety systems to prevent it. During the pre-flashover stage the fire can still be controlled, suppressed, and evacuation is still possible.

Although Computational Fluid Dynamics (CFD) based models can reproduce fire behavior to a considerable degree, the hand-calculation methods are still widely applied, since they are more time-efficient and cheaper when compared to numerical simulations and in general can provide a rough, but useful first estimate of the fire. Both, HGLT and interface height can be assessed through analytical equations (hand-calculation methods) or computational models (CFD), being HGLT the focus of the present work.

The McCaffrey, Quintiere and Harkleroad correlation [2] (known as MQH correlation) is considered the most well-established hand-calculation method to predict HGLT in pre-flashover compartment fires. However, this correlation was designed for fires positioned at the center of the room and on the ground level, which was proven to be the less hazardous condition. Nowadays, several other hand-calculation methods are available to predict fire safety parameters [2–5], but none of them takes into account the fire source location (walls proximity and vertical position) to determine the HGLT.

Several researchers have been analysing the influence of walls and corners on fire parameters, such as mass flow rate, HGLT and flame height [6–14]. Mowrer and Williamson [6] observed that fires positioned in corners and along walls have a restricted air entrainment and it results in higher HGLT than those predicted by

1 the MQH correlation. Consequently, they developed modification factors to adjust that correlation and extend its
2 applicability to wall and corner fires. Azhakesan *et al.* [10] undertook an experimental study of liquid pool fires
3 in corner and center fire geometries. In an initial interrogation they found out that the modifications to MQH
4 correlation suggested by Mowrer and Williamson [6] are reasonable. Some investigations about the influence of
5 the elevation of the fire source on fire parameters have been published. Backovski, Foote and Alvares [15]
6 investigated among other things, the effect of elevated fires on the temperature profiles in forced-ventilation
7 enclosure fires, observing that when the distance between the fire and the ceiling is shortened, the hotter become
8 the gas temperature. Mounaud [16] conducted experiments to analyse the influence of the elevation of the fire
9 source in compartment fires on the species generation and transport. Zhang *et al.* [17] conducted experiments
10 with elevated fires in closed compartments (to represent ship fires); they studied the smoke filling processes in
11 these cases, measuring parameters such as mass loss rate, light extinction coefficient, oxygen concentration and
12 gas temperature profile. In a posterior work, Zhang *et al.* [18] presented a similar investigation on a ceiling
13 vented compartment and observed that the fire location significantly impacted the light extinction coefficient, the
14 oxygen concentration and the gas temperature, producing a less hazardous fire if the fire was elevated higher,
15 which is the opposite behavior when comparing to elevated fires in closed compartments. Liu *et al.* [19]
16 conducted experiments to investigate the fire source elevation effect on fire and smoke behavior, focussing on
17 the critical velocity, in a tunnel with longitudinal ventilation. As can be seen, the literature is still very scarce on
18 this area.

19 In this work, new semi-empirical correlations are developed to predict the HGLT in pre-flashover
20 compartment fires as a function of the fire source location, heat release rate, ventilation factor, surface area,
21 effective heat transfer coefficient and ambient thermal properties. These correlations are based on numerical
22 experiments, performed with a widely validated CFD fire model (FDS). The main justification for choosing this
23 topic was the necessity of improvement on the hand-calculation methods to obtain pre-flashover compartment
24 fire parameters, to allow the fire safety engineers to obtain rapidly, more reliable data to design fire safety
25 systems. Knowing the HGLT helps engineers to predict the onset of flashover and to design fire suppression and
26 smoke detection/extraction systems, which give occupants more time to leave the fire compartment, saving lives.
27 Despite the existence of other hand-calculation methods to predict the HGLT, from the authors' best knowledge,
28 none of them take into account the position where the fire starts. Most of them were developed considering the
29 fire starting in the middle of the room, at the ground level and away from any objects that may restrict the air
30 entrainment into the flame. In this work we showed that this is the scenario which results in the lowest HGLT, so
31 the estimates obtained applying currently existing methods would probably underestimate the HGLT.

32 **2 Numerical experiments methodology**

33 A computational fluid dynamics (CFD) model namely Fire Dynamics Simulator (FDS) was applied to
34 simulate 252 pre-flashover compartment fire scenarios. These simulations reproduced the room geometry
35 applied on Steckler *et al.* [20–22], considering several fire source positions (longitudinal, transversal and
36 vertical).

37 FDS is a Large Eddy Simulation (LES) fire model, developed by the National Institute of Standards and
38 Technology (NIST) and VTT Technical Research Center of Finland, which solves numerically the Navier-
39 Stokes equations adapted for low-speed ($Ma < 0.3$). The core algorithm is an explicit predictor-corrector scheme,
40
41
42
43
44
45
46
47
48
49
50
51
52
53
54
55
56
57
58
59
60
61
62
63
64
65

second order accurate in space and time [23]. The FDS version employed in the simulations was the FDS 6.6.0 and its default models were applied.

Firstly, 13 cases in 15 different fire heat source positions at the ground level were tested to determine their influence on the temperature results. The tested fire positions can be seen in Figure 1(a) (indicated by the fuel pan position using letters A to Q) and the 13 studied cases are summarized in Table 1.

Based on the findings for the HGLT of the 15 fire source positions on ground level, 19 different elevations on the positions A, B and C were simulated (see Figure 1(b)). A total of 195 fire scenarios were simulated for the ground fire analysis, and 57 fire scenarios were simulated for the elevated fire source analysis, summing 252 numerical experiments.

A thermocouple tree in the front corner of the room measured the gas temperature profile (Figure 2). The thermocouple tree was placed 0.305 m from the walls, with the lower thermocouple 0.057 m from the floor and the other thermocouple spaced equally 0.114 m from each other. The HGLT (T_U) was obtained through the average value of the temperature in the upper portion of the room, above the temperature profile curve inflection.

The thermocouples were modelled to represent the characteristics of the physical ones in the experiments. The room geometry and the thermocouple tree can be seen in Figure 2.

All cases were simulated for 900 s, and reached steady state before 800 s, this means that the hot gas temperature did not change significantly with time anymore. The temperature results were obtained through an average considering the results obtained between 800 s and 900 s (steady state), to compensate the oscillatory results caused by the LES turbulence model.

2.1 Governing equations

The set of LES filtered equations which describe the fire phenomenon is composed by the Mass transport equation (Equation 1), the Species transport equation (2), the Momentum transport equation (3), the Energy (enthalpy) transport equation (Equation 4), and the equation of state, also known as ideal gas Law (Equation 5) [24].

$$\frac{\partial \bar{\rho}}{\partial t} + \nabla \cdot (\bar{\rho} \tilde{\mathbf{u}}) = \langle \dot{m}_b''' \rangle \quad (1)$$

$$\frac{\partial \bar{\rho} \tilde{Y}_i}{\partial t} + \nabla \cdot (\bar{\rho} \tilde{Y}_i \tilde{\mathbf{u}}) = -\nabla \cdot (\bar{J}_i + J_i^{sgs}) + \dot{m}_i''' + \langle \dot{m}_{b,i}''' \rangle_{vb} \quad (2)$$

$$\frac{\partial (\bar{\rho} \tilde{\mathbf{u}})}{\partial t} + \nabla \cdot (\bar{\rho} \tilde{\mathbf{u}} \tilde{\mathbf{u}}) = -\nabla \bar{p} - \nabla \cdot (\bar{\boldsymbol{\tau}} + \boldsymbol{\tau}^{sgs}) + \bar{\rho} \mathbf{g} + \langle \mathbf{f}_D''' \rangle_{vb} \quad (3)$$

$$\frac{\partial (\bar{\rho} \tilde{h})}{\partial t} + \nabla \cdot (\bar{\rho} \tilde{h} \tilde{\mathbf{u}}) = \frac{\bar{D} p_0}{\bar{D} t} - \nabla \cdot (\bar{\mathbf{q}} + \mathbf{q}^{sgs}) - \nabla \cdot \bar{\mathbf{q}}_r + \langle \dot{q}_{c,b}''' \rangle_{vb} + \langle \dot{h}_b''' \rangle_{vb} \quad (4)$$

$$\bar{\rho} = \frac{p_0 \bar{W}}{R \tilde{T}} \quad (5)$$

1 where ρ is the density, t is the time, \mathbf{u} is the velocity vector, \dot{m}_b''' is the source term of mass, Y_i is the mass
2 fraction of species i , J_i is the diffusive mass flux of species i , \dot{m}_i''' is the mass production rate per unit volume of
3 species i by chemical reactions, $\dot{m}_{b,i}'''$ is the mass production rate per unit volume of species i by evaporating
4 droplets/particles, p is the pressure, τ is the viscous stress tensor, \mathbf{g} is the gravity vector, f_b''' represents the drag
5 force per unit volume, h is the sensible enthalpy, p_0 is the thermodynamic pressure, \mathbf{q} is the heat flux vector, \mathbf{q}_r
6 is the radiative heat flux vector, $\dot{q}_{c,b}'''$ is the convective heat transfer source term of the fuel, \dot{h}_b''' is the fuel
7 enthalpy source term, T is the temperature, R is the universal gas constant, and \bar{W} is the molecular weight of the
8 gas mixture.

9 In FDS, the governing equations are approximated using finite differences on the uniformly spaced
10 three-dimensional numerical grid, since for LES models, uniform meshing is always preferred [25].

11 The solution of the momentum equation requires the solution of an elliptic partial differential equation
12 (PDE) for the pressure, so, before the components of velocity can be advanced in time, this elliptic PDE (known
13 as a Poisson equation) must be solved for the pressure term. It is solved using a direct Fast Fourier Transforms
14 (FFT) based solver that is part of a library of routines for solving elliptic PDEs called CRAYFISHPAK [25].

15 The turbulence model is based on Large Eddy Simulation (LES) and the subgrid-scale turbulent
16 viscosity, μ_t , is obtained with a modified Deardorff Model (FDS turbulence default model), given by:

$$17 \mu_t = \rho C_V \Delta \sqrt{k_{sgs}} \quad (6)$$

18 where ρ is the density, C_V is the model constant, set to the value $C_V = 0.1$, Δ is the width filter and k_{sgs} is the
19 subgrid kinetic energy.

20 In FDS, due to difficulties defining a consistent test filter for use with the Deardorff's turbulence model
21 near the wall, at corners, and inside cavities, the turbulent viscosity of the first off-wall cell is obtained from the
22 Smagorinsky model with Van Driest damping [25].

23 More information about the mathematical model solved by FDS can be found in McGrattan *et al.* [25].

24 2.2 Initial and boundary conditions

25 For the validation step, the initial ambient temperature (T_∞) was considered the same of the
26 experiments, varying for each case according to Steckler *et al.* [20]. However, after the validation step, for the
27 numerical experiments, the initial ambient temperature was specified as 24 °C (297 K) for all the cases, so the
28 HGLT could be analysed properly, once it depends on this initial condition. The initial and ambient pressure
29 (p_∞) was specified as 101,325 kPa for all the cases.

30 The lateral and top domain boundaries were assumed "OPEN", which means that the fluid is allowed to
31 enter or exit the computational domain based on local pressure gradients. The gradients of the tangential
32 components of velocity are set to zero at an open boundary.

33 The bottom domain boundary was assumed as a smooth solid insulated boundary (floor). The
34 compartment boundaries (walls and ceiling) were modelled as 0.1 m thick smooth solids with the properties
35 described in Table 2, which are based on the properties ranges described in [26]. These surfaces have insulation
36 characteristics of ceramic fiber boards and the back side of these wall obstructions was set as "EXPOSED",
37
38
39
40
41
42
43
44
45
46
47
48
49
50
51
52
53
54
55
56
57
58
59
60
61
62
63
64
65

1 allowing the model to compute the heat flux to, and temperature of, the walls.

2 For the modeling of boundary layer flows, FDS uses LES with near-wall modeling (wall functions)
3 [25]. The wall model used is the logarithmic law of the wall, so, the viscous stress at the wall, τ_w , is modeled
4 with a logarithmic velocity profile. In FDS, the law of the wall is approximated by:
5
6

$$7 \quad u^+ = y^+ \quad \text{for } y^+ < 11.81 \quad (7)$$

$$8 \quad u^+ = \frac{1}{\kappa} \ln y^+ + B \quad \text{for } y^+ \geq 11.81 \quad (8)$$

9
10
11
12
13
14
15
16 where $\kappa = 0.41$ is the von Kármán constant and $B = 5.2$. The friction velocity is defined as $u_\tau \equiv \sqrt{\tau_w/\rho}$, and
17 from the friction velocity the nondimensional streamwise velocity is defined as $u^+ \equiv u/u_\tau$ and the
18 nondimensional wall-normal distance is defined as $y^+ \equiv y/\delta_v$, where $\delta_v = \nu/u_\tau = \mu/(\rho u_\tau)$ and represents the
19 viscous length scale.
20
21

22 The fuel applied to all cases was methane with heat release rate (HRR) prescribed as constant,
23 according to Table 1. The data obtained through the present simulations was employed to analyze the influence
24 of the fire heat source location on the HGLT in pre-flashover compartment fires and to develop improved
25 correlations to predict this parameter.
26
27

28 2.3 Mesh resolution

29 Three different methods were applied to ensure that the proper mesh resolution was employed in the
30 numerical simulations. The first was the analysis of the non-dimensional parameter D^*/δ_x , largely employed for
31 FDS simulations; the second was a sensitivity analysis, and the third was the Measurement of the Turbulence
32 Resolution (MTR), which is the recommended method to verify the adequacy of the mesh resolution in LES
33 simulations [23, 27–29].
34
35
36
37
38

39 For simulations involving buoyant plumes, the non-dimensional parameter D^*/δ_x is a good way to
40 determine how well the flow field is resolved [30, 31]. D^* is the characteristic fire diameter given by Equation
41 (9) and δ_x is the nominal size of a mesh cell.
42
43
44

$$45 \quad D^* = \left(\frac{\dot{Q}}{\rho_\infty c_p T_\infty \sqrt{g}} \right)^{\frac{2}{5}} \quad (9)$$

46
47
48
49 where \dot{Q} is the HRR, ρ_∞ is the ambient air density, c_p in the ambient air specific heat, T_∞ is the ambient
50 temperature and g is the acceleration of gravity.
51
52

53 As a Rule of Thumb, McDermott *et al.* [29] suggests that values of D^*/δ_x of the order of 10 provide an
54 adequate grid resolution for the plume, while the validation study sponsored by the U.S. Nuclear Regulatory
55 Commission [32], suggested D^*/δ_x values ranging from 4 to 16.
56
57

58 Table 3 presents the values of D^* and D^*/δ_x for four mesh sizes ($\delta_x = 6$ cm, 5 cm, 4 cm and 3 cm).
59 These meshes are equally spaced in all directions x - y - z , and they are uniform all over the computational domain.
60 As can be observed in Table 3, all meshes present D^*/δ_x contained inside the recommended range.
61
62
63
64
65

1 The second criteria used to evaluate the mesh discretization was a comparison between the results
 2 (temperature profiles, average hot gas layer temperature T_U , average lower layer temperature T_L and
 3 computational time) obtained for the four different meshes applied to test 14 from Steckler *et al.* [20] (according
 4 to Table 6). The results are shown in Figure 3 and Table 4.
 5
 6

7 As can be observed in Figure 3 and Table 4, meshes $\delta_x = 5$ cm, 4 cm and 3 cm present similar results,
 8 all of them agreeing well with the experimental data. So, the mesh $\delta_x = 5$ cm has been chosen to be applied for
 9 the numerical experiments, as a matter of computational time and result stability.
 10

11 To ensure the right selection of the mesh, the MTR for the 5 cm mesh has been calculated for cases 5,
 12 11, 12 and 13 (described in Table 1). The MTR is a posteriori analysis that gives a measure of how well the
 13 turbulence is being resolved in the domain in LES simulations. It is a scalar quantity defined locally by Equation
 14 (10).
 15
 16
 17

$$18 M(x) = \frac{\langle k_{sgs} \rangle}{\langle TKE \rangle + \langle k_{sgs} \rangle} \quad (10)$$

19 where the angled brackets denote a time-average, the resolved turbulent kinetic energy per unit mass (TKE) is
 20 given by Eq. (11) and the subgrid kinetic energy (k_{sgs}) is obtained directly from FDS for each point of interest.
 21
 22

$$23 TKE = \frac{1}{2} ((\tilde{u} - \langle \tilde{u} \rangle)^2 + (\tilde{v} - \langle \tilde{v} \rangle)^2 + (\tilde{w} - \langle \tilde{w} \rangle)^2) \quad (11)$$

24 where \tilde{u} , \tilde{v} , \tilde{w} are the resolved LES velocity components and are also obtained from FDS. The MTR value was
 25 calculated based on 15 points measured in regions of interest inside the compartment. The results presented in
 26 Table 5 are the mean MTR values.
 27
 28

29 According to Pope [27], the MTR value must be less than or equal to 0.2, which corresponds to the
 30 resolution of 80% of the turbulent kinetic energy. Additionally, as showed by McDermott [29], a MTR mean
 31 value near 0.2 provides satisfactory results for mean velocities and species concentrations in non-reacting,
 32 buoyant plumes. So, the 5 cm size mesh is capable to resolve more than 80% of the kinetic energy of the flow
 33 field.
 34

35 2.4 Comparison with Experimental Data

36 To validate the numerical model, the results of HGLT (T_U) were compared to experimental data
 37 presented by Steckler *et al.* [20] for 40 fire scenarios. The description of the investigated scenarios and its results
 38 can be seen in Table 6. On experiments 160, 163 and 164 the fire sources were raised 0.3 m from the floor, while
 39 it was on the ground for the other experiments.
 40
 41

42 As can be observed in Table 6, the numerical model can be considered validated, since for the HGLT
 43 the maximum relative deviation found was 13.98% and the mean relative error was 3.17%,
 44

45 The comparison between experimental temperature profiles and the ones obtained by FDS for tests 14,
 46 160, 410, 163, 610 and 164 can be seen in Figure 4. Similar results were obtained for all 40 tests described in
 47 Table 6. A good agreement between experimental data and numerical results was found, so it can be concluded
 48 that the mathematical model employed on FDS was validated and can be applied to generate reliable data for
 49 pre-flashover compartment fire scenarios.
 50
 51
 52
 53
 54
 55
 56
 57
 58
 59
 60
 61
 62
 63
 64
 65

3 RESULTS AND DISCUSSIONS

3.1 Fire Source Position Influence: ground level

The influence of the fire source location at the ground level was analysed varying the fire position along the axis x (longitudinal direction) and y (transversal direction), as shown in Figure 1(a). The 13 studied cases (Table 1) have been simulated in 15 different positions (Figure 1(a)), resulting 195 different scenarios.

The numbers inside the circles in Figures 5(a)-(f) show the HGLT (T_U) obtained through FDS simulations for each one of the studied ground level positions (Letters A to Q in Figure 1(a)) for cases 1, 5, 9, 11, 12 and 13 (according to Table 1). Each plot (a to f) represent the upper view of the room for the indicated cases and the HGLT (T_U) results were placed on the position inside the room where the fire source was placed (these temperatures must be assumed as homogeneous over all the HGL), so each square (plots a to f) presents the condensed results of the 15 tested fire positions (Figure 1(a)).

As can be observed, the highest HGLT were found for the corner fire locations (positions B and N), represented by the red circles, followed by the near wall fire location (positions C, D, E, H and K) represented by the yellow circles. The positions away from walls (center positions - A, F, G, J, L, M, P and Q), represented by the green circles, are the ones which produced the lowest HGLT, especially those near the opening doorway. This behaviour was expected since corner and wall fires are subjected to reduced air entrainment.

According to Zukoski *et al.* [33], in the early stages of a fire (pre-flashover) in a building, the rate of production of hot gases by a fire and the temperature of these gases will depend very strongly on the rate of entrainment in the fire plume and in the flame itself. According to Mowrer and Williamson [6], the fire plume temperature will significantly increase for corner and near wall fire plumes; they stated that the convective energy flux through the openings would not depend on the fire source location in the room. This statement was confirmed by the results shown in Figures 5(a)-(f), once fire source position in the same group of interest (away from walls (center), along walls or near corners) showed small variations.

An interesting observation can be made through Figure 5(c), which represents case 9 (window opening). For the window cases (cases 8, 9 and 10), when the fire source is in position Q (Figure 1(a)), the upper layer temperature is higher than the other center positions (green circles), this is different from the cases with a doorway, which presented the lowest HGLT when the fire source was in position Q. This is explained by the reduction of air entrainment caused by the presence of the wall in the lower part of the fire source in the window cases for position Q. Another pattern can be observed, once the ventilation factor (opening size) is augmented, lower become the HGLT for each fire position.

So, from this analysis, we can conclude that what causes the increase in the HGLT is the presence of an obstruction, that can be the walls or even a piece of furniture, which restricts the air entrainment into the flame. This confirmed a weak influence of the fire source location for the cases when the fire source is at the floor level and at the same position group (away from walls (center), along walls or near corners), as suggested by Mowrer and Williamson [6].

3.2 Fire Source Position Influence: elevated fire

For analysing the influence of the vertical position of the fire source on the HGLT, 19 elevations (ranging from $z = 0$ m to $z = 1.8$ m with 0,1 m increments) have been simulated for positions A (center fire), B

1 (corner fire) and C (back-wall fire), as can be seen in Figure 1(a). These simulations were conducted only for
2 case 5 (Table 1), generating data for 57 numerical simulations.
3

4 Figure 6 presents the results obtained from these numerical experiments for the HGLT as a function of
5 the fire source elevation (z) for positions A, B and C.
6

7 As can be observed, as the height of the fire source location was augmented, so was the HGLT. This
8 behaviour was observed for all positions (center, wall and corner fires). However, the influence of the elevation
9 was greater for fires in the center of the room, followed by fires along walls, and finally fires near corners. This
10 may be explained by the reduction of the air entrainment rate. When the fire source is elevated, it becomes closer
11 to the hot gas layer interface and its plume and flame have a smaller region to entrain fresh air (Figures 7(a)-(c)).
12 With this reduction of air entrainment, the HGLT rises. Once, fires in corners and along walls already have an
13 reduced air entrainment of approximately one quarter and one half (as a consequence of the walls restriction in
14 the perimeter of the flame/plume), respectively, when elevated they suffer less influence than the ones away
15 from walls.
16
17
18
19
20

21 Significant differences in the HGLT between subsequent levels (elevations) were observed, being most
22 of them of the order of 10-20 °C (considering increasing steps of $\Delta z = 0.1$ m between elevations), while when
23 comparing HGLT for the fire source at the floor level and at the highest studied level ($z = 1.8$ m), the difference
24 in the HGLT were of 110°C when the fire is placed in a corner, 180°C when the fire is placed near a wall and 242
25 °C when the fire is placed in the center of the room.
26
27

28 Although the influence of the elevation on the HGLT is not perfectly linear, a linear dependence can be
29 considered to correlate the HGLT and the elevation of the fire source.
30
31

32 3.3 *Semi-empirical Correlations to Predict HGLT considering the fire position*

33 As it can be observed in the previous analysis, the fire source location has an important influence on the
34 HGLT. It is noticed that walls or other objects adjacent to the fire will cause an augmentation on the plume
35 temperature, and consequently in the HGLT. It is also noticed the great influence that the vertical fire source
36 position has on the HGLT, which follows a quite linear trend.
37
38
39

40 As the available correlations in the literature do not take into account properly the fire source location,
41 the present work developed improved semi-empirical correlations to predict the HGLT in pre-flashover
42 compartment fires, depending on the fire position. As well as the MQH correlation [2], the present correlations
43 were derived from an energy balance on the well-stirred gas layer in the upper portion of the room, resulting in a
44 function of two dimensionless terms presented in Equation 12.
45
46
47
48

$$49 \frac{\Delta T}{T_{\infty}} = f \left(\frac{\dot{Q}}{\sqrt{g C_p \rho_{\infty} T_{\infty} A_0 \sqrt{H_0}}}, \frac{h_k A_T}{\sqrt{g C_p \rho_{\infty} A_0 \sqrt{H_0}}} \right) \quad (12)$$

50 where ΔT corresponds to the upper layer temperature rise ($\Delta T = TU - T_{\infty}$), the first term in parenthesis
51 represents the ratio of the energy released by the fire to the energy convected through the openings, and the
52 second term stands for the energy lost through the walls divided by the energy convected. Where \dot{Q} is the HRR
53 [kW], g is the acceleration of gravity [m/s^2], C_p is the specific heat of the ambient air [$kJ/(kg \cdot K)$], ρ_{∞} is the
54 density of the ambient air [kg/m^3], T_{∞} is the ambient air temperature [K], $A_0 \sqrt{H_0}$ is the ventilation factor [$m^{5/2}$],
55
56
57
58
59
60
61
62
63
64
65

h_k is the effective heat transfer coefficient [kW/(m² · K)] and A_T is the total area of the compartment surface [m²]. These are the same dimensionless variables employed in the MQH correlation [2], however, the MQH correlation was developed only considering fires at the center of the room, and does not account for the fire source elevation effect on the HGLT.

The effective heat transfer coefficient must be obtained in the same manner that in the MQH correlation [2], depending on the exposure time (t) and thermal penetration time (t_p) of the wall, which is given by $t_p = \delta_w^2 / (4\alpha_w)$, where α_w is the wall thermal diffusivity [m²/s] and δ_w is the wall thickness [m]. For exposure time smaller than the penetration time ($t < t_p$), the effective heat transfer coefficient is given by $h_k = \sqrt{k\rho c/t}$ while for an exposure time larger than the penetration time ($t > t_p$), it is $h_k = k/\delta_w$, where k is the wall thermal conductivity [kW/(m · K)], ρ is the wall density [kg/m³], c is the specific heat of the wall [kJ/(kg · K)].

Figure 8 shows the dimensionless temperature ($\Delta T/T_\infty$) obtained by FDS for all the ground level simulations as a function of the first (Fig. 8(a)) and second (Fig. 8(b)) dimensionless terms in parenthesis in Equation 12, showing a power law relationship, so Equation 12 can assume the functional form presented in Equation 13.

$$\frac{\Delta T}{T_\infty} = \gamma \left(\frac{\dot{Q}}{\sqrt{g} C_p \rho_\infty T_\infty A_0 \sqrt{H_0}} \right)^\alpha \cdot \left(\frac{h_k A_T}{\sqrt{g} C_p \rho_\infty A_0 \sqrt{H_0}} \right)^\beta \quad (13)$$

where the constant γ and the exponents α and β are determined from a best fit of the data from each group of fire positions (center, wall and corner) at the ground level, since it was observed a great influence of these fire positions on the HGLT. This means that 3 variants of the correlation are obtained for the HGLT prediction, one for each position of the fire source.

The influence of the fire elevation on the HGLT did not show a power law relation, but a linear tendency instead. These effects then considered as a correction term (δ) summed to the HGLT correlation when the elevation is different from zero, according to Equation 14.

$$\frac{\Delta T}{T_\infty} = \gamma \left(\frac{\dot{Q}}{\sqrt{g} C_p \rho_\infty T_\infty A_0 \sqrt{H_0}} \right)^\alpha \cdot \left(\frac{h_k A_T}{\sqrt{g} C_p \rho_\infty A_0 \sqrt{H_0}} \right)^\beta + \delta \quad (14)$$

This correction term (δ) is defined using the dimensionless parameter z^* :

$$z^* = \frac{z}{H} \quad (15)$$

where z is the vertical fire position in m and H is the height of the room in m .

The correlation of the correction term (δ) for Equation 14 was obtained through a simple linear regression of the difference between the dimensionless temperature at each level $(\Delta T/T_\infty)_{level}$ and at the ground level $(\Delta T/T_\infty)_{ground}$.

The fitting of the data for terms α , β and γ was obtained through the software SPSS applying a multiple linear regression.

1 Three different sets of coefficients for the correlation (Equation 14) were obtained according to the fire
2 position inside the room (away from walls, near a corners and near a wall), see Table 7. Observe that the term δ
3 must be set as zero if the fire occurs at the ground level ($z = 0$), while if the fire is elevated, it must be calculated
4 according to its dimensionless height (z^*). All the temperatures in the correlation (Eq. 14) must be entered as
5 absolute temperatures [K], so the HGLT (TU) obtained through the use of this correlation will also be given in
6 K, but can easily be converted to $^{\circ}\text{C}$.
7
8
9

10 Figure 9 presents a comparison between the predicted values of the HGLT applying Equation 14 with
11 the coefficients presented in Table 7 against the numerical data obtained with FDS. As FDS provides all
12 temperatures in $^{\circ}\text{C}$, the temperatures obtained through the correlations were also converted from K to $^{\circ}\text{C}$. The
13 dashed lines represent a 10% tolerance. As can be observed, an excellent fitting was obtained applying the newly
14 developed correlation for all the fire positions.
15
16
17
18

19 3.4 External validation of the new semi-empirical correlations: comparison with experimental data

20 To ensure the quality and applicability of the newly obtained correlations, the predictions obtained from
21 Equation 14 with the coefficients from Table 7 are then compared to different sets of experimental data available
22 in the literature, to represent several fire scenarios, different from those employed to fit the new correlation.
23
24

25 Table 8 describe the characteristics of each experimental data set employed in the external validation
26 (for more information about the fire scenarios, the references must be consulted).
27

28 Figures 10(a)-(c) show the comparison of the HGLT predicted with the new correlation and the
29 experimental data for fires away from walls (center), near corners and near walls, respectively. The continuous
30 line represents that the predicted HGLT values are equal to the experimental ones, while the dashed lines
31 represent a 10% tolerance.
32
33

34 As can be observed in Figure 10(a), even with a great variety of fire scenarios, an excellent agreement
35 was obtained for most of the experimental data. A slight less precise agreement was found to Johansson *et al.*
36 [32], where the predicted results were found to be a bit lower than the experiments. This may be explained by the
37 fact that these data were obtained from a multi-room experiment, where the fire room opening was connected to
38 another room instead of being connected to the exterior environment. This usually reduces the flow of air into
39 and out the room, which in turn, increases the upper layer temperature.
40
41
42

43 In Figure 10(b), a very good agreement was obtained for experimental data from McCaffrey and
44 Rockett [35], Li and Hertzberg [36], and Steckler's experiments [20]. The data from Mowrer and Williamson
45 [6], showed a slight higher variation, but still of the order of 20%, which is still a very reasonable agreement,
46 considering that experimental data always present some measurement uncertainty and that there was a lack of
47 information about the ambient temperature during experiments and precise wall and linen material properties
48 that had to be estimated to apply in the correlation.
49
50
51

52 As can be seen in Figure 10(c), a very good agreement was obtained for most of the experimental data,
53 most of them showing differences smaller than 10%. The highest differences were found for very wide line fire
54 source (from Quintiere *et al.* [37]), which may be expected, once the correlation was designed with data from
55 circular burners, and again for the data from Mowrer and Williamson [6], which can be related as discussed
56 before to the experimental uncertainty or even to the lack of information.
57
58
59

60 Although the numerical results applied to develop the correlation presented small heat release rates,
61
62
63
64
65

1 which would represent the maximum heat release rate of a small pool fire (31.6 and 62.9 kW) or small wood
2 furniture (105.3 and 158 kW) (e.g. a wood framed chair with Polyurethane foam and cover), the comparison to
3 other sets of experiments showed that these newly developed correlations stand for higher heat release rates as
4 well as to different fire scenarios, including room sizes, ventilation factors, construction materials, etc.
5
6

7 8 **4 Conclusions** 9

10
11 In this work numerical experiments were performed using the software FDS, in order to study the
12 influence of the fire source position (transversal, longitudinal and vertical directions) on the upper layer
13 temperature for pre-flashover compartment fires. It was confirmed that the HGLT does not depend on the fire
14 source position when the fire occurs away from walls or obstructions (i.e. pieces of furniture), and that there is
15 an augmentation on those temperatures when the fire occurs at corners or walls (at the ground level). Fires near
16 corners presented the highest temperatures, followed by near wall fires, and the lowest temperatures were
17 observed for fire sources away from walls.
18
19

20
21 The present paper also showed a great influence of the fire source elevation on the HGLT. An increase
22 on the HGLT, mostly on the range of 10-20 °C, was observed between subsequent vertical levels ($\Delta z = 0.1$ m),
23 while when comparing the HGLT for the fire source at the floor level ($z = 0$ m) and at the highest level ($z = 1.8$
24 m) the difference in the HGLT was of more than 100 °C in all cases, reaching 242 °C for the fire at the center of
25 the room. It was also observed that fires away from obstructions or walls suffered more influence from the
26 elevation of the fire source, followed by fires near wall and the lowest influence was presented by fires near
27 corners. It was noted that for fires occurring near the ceiling (above 50-55% the room high) the behaviour was
28 the opposite than for fires on the floor, presenting the highest temperatures for fires at the center and the lowest
29 for fires near corners.
30
31

32
33 Based on these findings, improved correlations have been designed to predict the HGLT, considering
34 the fire source position. The correlations were developed based on numerical data generated using the software
35 FDS. A good agreement between the HGLT predicted by the newly developed correlations and the numerical
36 data from FDS have been found. As an external validation, predictions from the newly developed correlations
37 were also compared to experimental data from different fire scenarios, showing a good agreement. So, the new
38 correlations can be considered as validated for pre-flashover compartment fires and are capable to predict the
39 upper layer temperature considering the fire source location (including its vertical position). This is an important
40 achievement once it was observed that fires near corner or at higher elevations produce higher upper layer
41 temperatures than those at the ground and away from walls, which are the ones predicted by the conventional
42 correlations previously available in the literature.
43
44
45
46
47
48
49
50
51

52 **Acknowledgements:** 53

54
55 This study was financed in part by the Coordenação de Aperfeiçoamento de Pessoal de Nível Superior –
56 Brasil (CAPES) – Finance Code 001.
57

58 Author FRC thanks CNPq/Brazil for research grant 400472/2016-3.
59

60 Authors also thank UFRGS for the SPSS software license.
61
62
63
64
65

References

1. Dusso A, Grimaz S, Salzano E (2016) Quick assessment of the hot gas layer temperature and potential fire spread between combustible items in a confined space. *Chem Eng Trans* 53:37–42. <https://doi.org/10.3303/CET1653007>
2. McCaffrey BJ, Quintiere JG, Harkleroad MF (1981) Estimating room temperatures and the likelihood of flashover using fire test data correlations. *Fire Technol* 17:98–119. <https://doi.org/10.1007/BF02479583>
3. Tlili O, Mhiri H, Bournot P (2016) Empirical correlation derived by CFD simulation on heat source location and ventilation flow rate in a fire room. *Energy Build* 122:80–88. <https://doi.org/10.1016/j.enbuild.2016.04.028>
4. Delichatsios MA, Lee YP, Tofilo P (2009) A new correlation for gas temperature inside a burning enclosure. *Fire Saf J* 44:1003–1009. <https://doi.org/10.1016/j.firesaf.2009.06.009>
5. Matsuyama K, Fujita T, Kaneko H, et al (1998) Simple predictive method for room fire behaviour.pdf. *Fire Sci Technol* 18:23–32. <https://doi.org/10.3210/fst.18.23>
6. Mowrer FW, Williamson RB (1987) Estimating room temperatures from fires along walls and in corners. *Fire Technol* 23:133–145. <https://doi.org/10.1007/BF01040428>
7. Tran HC, Janssens ML (1991) Wall and Corner Fire Tests on selected Wood Products. *J Fire Sci* 9:106–124. <https://doi.org/10.1177/073490419100900202>
8. Takahashi W, Tanaka H, Sugawa O, Ohtake M (1997) Flame and Plume Behavior in and near a Corner of Walls. *Fire Saf Sci Fifth Int Symp* 261–271. <https://doi.org/10.3801/IAFSS.FSS.5-261>
9. Poreh M, Garrad G (2000) Study of wall and corner fire plumes. *Fire Saf J* 34:81–98. [https://doi.org/10.1016/S0379-7112\(99\)00040-5](https://doi.org/10.1016/S0379-7112(99)00040-5)
10. Azhakesan MA, Shields TJ, Silcock GWH, Quintiere JG (2003) An interrogation of the MQH correlation to describe centre and near corner pool fires. *Fire Saf Sci* 371–382. <https://doi.org/10.3801/IAFSS.FSS.7-371>
11. Gao ZH, Ji J, Fan CG, et al (2014) Influence of sidewall restriction on the maximum ceiling gas temperature of buoyancy-driven thermal flow. *Energy Build* 84:13–20. <https://doi.org/10.1016/j.enbuild.2014.07.070>
12. Gao ZH, Ji J, Fan CG, et al (2016) Determination of smoke layer interface height of medium scale tunnel fire scenarios. *Tunn Undergr Sp Technol* 56:118–124. <https://doi.org/10.1016/j.tust.2016.02.009>
13. Ji J, Fu Y, Li K, et al (2015) Experimental study on behavior of sidewall fires at varying height in a corridor-like structure. *Proc Combust Inst* 35:2639–2646. <https://doi.org/10.1016/j.proci.2014.06.041>
14. Węgrzyński W, Konecki M (2018) Influence of the fire location and the size of a compartment on the heat and smoke flow out of the compartment. *AIP Conf Proc* 1922:. <https://doi.org/10.1063/1.5019110>
15. Backovsky J, Foote KL, Alvares NJ (1989) Temperature Profiles in Forced-Ventilation Enclosure Fires. *Fire Saf Sci —Proceedings Second Int Symp* 315–324. <https://doi.org/10.3801/IAFSS.FSS.2-315>
16. Mounaud LG (2004) A Parametric Study of the Effect of Fire Source Elevation in a Compartment
17. Zhang J, Lu S, Li Q, et al (2012) Smoke filling in closed compartments with elevated fire sources. *Fire Saf J* 54:14–23. <https://doi.org/10.1016/j.firesaf.2012.08.003>

18. Zhang J, Lu S, Li Q, et al (2013) Experimental study on elevated fires in a ceiling vented compartment. *J Therm Sci* 22:377–382. <https://doi.org/10.1007/s11630-013-0639-5>
19. Liu Y, Fang Z, Tang Z, et al (2020) Analysis of experimental data on the effect of fire source elevation on fire and smoke dynamics and the critical velocity in a tunnel with longitudinal ventilation. *Fire Saf J* 114:103002. <https://doi.org/10.1016/j.firesaf.2020.103002>
20. Steckler KD, Quintiere JG, Rinkinen WJ (1982) Flow Induced by Fire in a Compartment
21. Steckler KD, Baum HR, Quintiere JG (1984) Fire Induced Flows Through Room Openings - Flow Coefficients
22. Steckler KD, Baum HR, Quintiere JG (1984) Fire induced flows through room openings-flow coefficients. *Symp Combust* 20:1591–1600. [https://doi.org/10.1016/S0082-0784\(85\)80654-8](https://doi.org/10.1016/S0082-0784(85)80654-8)
23. McGrattan K, Hostikka S, McDermott R, et al (2020) Sixth Edition Fire Dynamics Simulator User 's Guide (FDS). NIST Spec Publ 1019 Sixth Edit:
24. Mell W, Maranghides A, McDermott R, Manzello SL (2009) Numerical simulation and experiments of burning douglas fir trees. *Combust Flame* 156:2023–2041. <https://doi.org/10.1016/j.combustflame.2009.06.015>
25. McGrattan K, Hostikka S, Floyd J, et al (2020) Fire Dynamics Simulator Technical Reference Guide Volume 1: Mathematical Model (Sixth Edition). Gaithersburg, MD
26. Fryatt J (1976) Basic properties of ceramic fibres and their effect on insulation performance. *Appl Energy* 2:117–126. [https://doi.org/10.1016/0306-2619\(76\)90031-3](https://doi.org/10.1016/0306-2619(76)90031-3)
27. Pope SB (2004) Ten questions concerning the large-eddy simulation of turbulent flows. *New J Phys* 6:. <https://doi.org/10.1088/1367-2630/6/1/035>
28. McDermott RJ (2011) Quality Assessment in the Fire Dynamics Simulator : a Bridge To Reliable Simulations. Fire Evacuation Model Tech Conf 2011
29. McDermott RJ, Forney GP, McGrattan K, Mell WE (2010) FIRE DYNAMICS SIMULATOR VERSION 6: COMPLEX GEOMETRY, EMBEDDED MESHES, AND QUALITY ASSESSMENT. In: V European Conference on Computational Fluid Dynamics ECCOMAS CFD. Lisbon, Portugal, pp 14–17
30. McGrattan K, Hostikka S, McDermott R, et al (2017) Fire Dynamics Simulator User's Guide. Gaithersburg, MD
31. McGrattan K, Hostikka S, McDermott R, et al (2017) Fire Dynamics Simulator Technical Reference Guide Volume 3: Validation. Gaithersburg, MD
32. Salley MH, Kassawara RP (2007) Verification and Validation of Selected Fire Models for Nuclear Power Plant Applications, Volume 7: Fire Dynamics Simulator (FDS), U.S. Nuclear Regulatory Commission, Office of Nuclear Regulatory Research (RES), Rockville, MD,. and Electric Power Research Institute (EPRI), Palo Alto, CA, NUREG- 1824 and EPRI 1011999.
33. Zukoski EE, Kubota T, Cetegen B (1981) Entrainment in fire plumes. *Fire Saf J* 3:107–121. [https://doi.org/10.1016/0379-7112\(81\)90037-0](https://doi.org/10.1016/0379-7112(81)90037-0)
34. Johansson N, Svensson S, Van Hees P (2015) An evaluation of two methods to predict temperatures in multi-room compartment fires. *Fire Saf J* 77:46–58. <https://doi.org/10.1016/j.firesaf.2015.07.006>
35. McCaffrey BJ, Rockett J a. (1977) Static pressure measurements of enclosure fires. *J Res Natl Bur Stand*

1 (1934) 82:107–117. <https://doi.org/10.6028/jres.082.009>

- 2
3 36. Li YZ, Hertzberg T (2015) Scaling of internal wall temperatures in enclosure fires. *J Fire Sci* 33:113–
4 141. <https://doi.org/10.1177/0734904114563482>
5
6 37. Quintiere JG, Steckler K, Corley D (1984) An assessment of fire induced flows in compartments. *Fire*
7 *Sci. Technol.* 4:1–14
8
9 38. Hamins A, Maranghides A, Johnsson R, et al (2006) Report of Experimental Results for the International
10 Fire Model Benchmarking and Validation exercise # 3. NIST Spec Publ 1013:
11
12 39. Johansson N, Svensson S, van Hees P (2015) A Study of Reproducibility of a Full-Scale Multi-Room
13 Compartment Fire Experiment. *Fire Technol* 51:645–665. <https://doi.org/10.1007/s10694-014-0408-3>
14
15 40. Dembsey NA, Pagni PJ, Williamson RB (1995) Compartment fire experiments: Comparison with
16 models. *Fire Saf J* 25:187–227. [https://doi.org/10.1016/0379-7112\(96\)00002-1](https://doi.org/10.1016/0379-7112(96)00002-1)
17
18
19
20
21
22
23
24
25
26
27
28
29
30
31
32
33
34
35
36
37
38
39
40
41
42
43
44
45
46
47
48
49
50
51
52
53
54
55
56
57
58
59
60
61
62
63
64
65

Table 1. List of openings and HRRs employed in the simulations

#	Opening size (W × H)	HRR [kW]
1	2/6 door (0.24 m × 1.83 m)	62.9
2	3/6 door (0.36 m × 1.83 m)	62.9
3	4/6 door (0.49 m × 1.83 m)	62.9
4	5/6 door (0.62 m × 1.83 m)	62.9
5	6/6 full door (0.74 m × 1.83 m)	62.9
6	7/6 door (0.86 m × 1.83 m)	62.9
7	8/6 door (0.99 m × 1.83 m)	62.9
8	3/3 full window (0.74 m × 1.38 m)	62.9
9	2/3 window (0.74 m × 0.92 m)	62.9
10	1/3 window (0.74 m × 0.46 m)	62.9
11	6/6 full door (0.74 m × 1.83 m)	31.6
12	6/6 full door (0.74 m × 1.83 m)	105.3
13	6/6 full door (0.74 m × 1.83 m)	158

Table 2. Walls and ceiling properties

Material	Density [kg/m ³]	Heat capacity [J/(kg·K)]	Thermal conductivity [W/(m·K)]
Ceramic fiber board	260	1000	0.08

Table 3. Values of D^* and D^*/δ_x for meshes 6 cm, 5 cm, 4 cm and 3 cm

HRR (kW)	D^*	D^*/δ_x			
		$\delta_x = 6$ cm	$\delta_x = 5$ cm	$\delta_x = 4$ cm	$\delta_x = 3$ cm
31.60	0.24	4.02	4.83	6.03	8.04
62.90	0.32	5.29	6.35	7.94	10.58
105.30	0.39	6.51	7.81	9.76	13.01
158.00	0.46	7.65	9.19	11.48	15.31

Table 4. Mesh sensitivity analysis and computational time

Mesh size	T_U [°C]	T_L [°C]	Time [h]
$\delta_x = 6$ cm	115.6	50.49	30.29
$\delta_x = 5$ cm	124.82 (7.4%)	52.72 (4.3%)	54.97
$\delta_x = 4$ cm	126.29 (1.2%)	52.59 (0.2%)	138.12
$\delta_x = 3$ cm	128.55 (1.8%)	51.94 (1.3%)	227.02

Table 5. MTR results for mesh size $\delta_x = 5$ cm

#	Fire position	HRR [kW]	MTR [5 cm]
5	A	62.90	0.159
11	A	31.60	0.173
12	A	105.30	0.140
13	A	158.00	0.137

Table 6. Comparison between numerical (FDS, present study) and experimental (Steckler *et al.* [20]) results

Test ²	Opening ³	HRR (kW)	Fire position	T_{∞} [°C]	T_U (Exp) [°C]	T_U (FDS) [°C]	Relative Dev. [%]
10	2/6	62.9	A	26	190	203.61	-7.16
11	3/6	62.9	A	28	164	154.29	5.92
12	4/6	62.9	A	22	141	134.98	4.27
13	5/6	62.9	A	23	129	126.72	1.77
14	6/6	62.9	A	29	129	126.85	1.67
16	7/6	62.9	A	26	120	113.72	5.23
17	8/6	62.9	A	22	109	102.54	5.93
22	Full Win.	62.9	A	30	143	145.69	-1.88
23	2/3 Win.	62.9	A	26	177	181.43	-2.50
41	1/3 Win.	62.9	A	16	270	259.62	3.84
19	6/6	31.6	A	29	86	86.13	-0.15
20	6/6	105.3	A	35	183	187.78	-2.61
21	6/6	158	A	36	243	244.83	-0.75
160	6/6	62.9	Ar ¹	6	136	126.66	6.87
114	2/6	62.9	B	32	248	253.54	-2.23
144	3/6	62.9	B	30	216	215.36	0.30
212	4/6	62.9	B	24	194	193.87	0.07
242	5/6	62.9	B	29	197	192.48	2.29
410	6/6	62.9	B	21	181	177.71	1.82
240	7/6	62.9	B	29	179	173.51	3.07
116	8/6	62.9	B	29	172	167.29	2.74
122	Full Win.	62.9	B	28	194	199.64	-2.91
224	2/3 Win.	62.9	B	26	216	222.05	-2.80
220	6/6	31.6	B	26	118	120.94	-2.49
221	6/6	105.3	B	27	234	251.18	-7.34
163	6/6	62.9	Br ¹	6	190	183.35	3.50
514	2/6	62.9	C	9	209	204.73	2.04
544	3/6	62.9	C	7	173	163.15	5.69
512	4/6	62.9	C	21	173	169.25	2.17
542	5/6	62.9	C	20	160	157.42	1.61
610	6/6	62.9	C	18	152	153.6	-1.05
540	7/6	62.9	C	14	140	135.28	3.37
517	8/6	62.9	C	15	134	131.76	1.67
622	Full Win.	62.9	C	10	153	156.29	-2.15
524	2/3 Win.	62.9	C	9	178	175.88	1.19
541	1/3 Win.	62.9	C	8	288	265.58	7.78
520	6/6	31.6	C	18	94	95.08	-1.15
521	6/6	105.3	C	14	207	207.79	-0.38
513	6/6	158	C	16	289	288.1	0.31
164	6/6	62.9	Cr ¹	7	161	138.5	13.98

¹ r represents the fire source locations raised 0.3 m from the floor level.

² Test numeration is in accordance with Steckler *et al.* [20].

³ Opening codes (e.g. 2/6, 3/6, 1/3, etc.) can be seen in Table 1

Table 7. Coefficients for the new correlation (Equation 14)

Fire position	α	β	γ	δ^1
Away from walls (center)	0.8	-0.33	1.55	$0.99z^*-0.03$
Near a corner	0.76	-0.48	1.26	$0.47z^*+0.02$
Near walls	0.79	-0.47	1.26	$0.83z^*-0.08$

¹ If the fire occurs in the ground level ($z=0$), the correction term δ must be considered zero.

Table 8. Experimental data sets employed in the external validation of the new correlation.

Experimental Data Set	Multi-room	Fire room size (W x L x H) [m]	Openings (Wo x Ho) [m]	HRR	Fire location
Hamins et al. (2006) [38]	No	7.04×21.7×3.82	Door (2.0×2.0)	1 MW	Center at ground
Johansson et al. (2015) [39]	Yes	1.2×1.2×0.8 0.6×0.9×0.6	Door (0.2×0.5) Door (0.3×0.5)	10 kW 20 kW	Center at ground
Quintiere et al. (1984) [37]	No	2.8×2.8×2.13	Door (0.23×1.83) Door (0.49×1.83) Door (0.74×1.83) Door (0.99×1.83) Window (0.74×1.37) Window (0.74×0.91) Window (0.74×0.46)	From 30 to 120 kW	Wall at ground
Dembsey et al. (1995) [40]	No	2.5×3.7×2.5	Door (0.76×2.0)	From 330 to 980 kW	Center elevated 0.61 m Wall elevated 0.61 m
Li and Hertzberg (2015) [36]	No	2.4×2.4×3.6	Door (0.8×2.0)	100 kW 300 kW	Center elevated 0.3 m Corner elevated 0.3 m
McCaffrey and Rockett (1977) [35]	No	3.0×3.0×2.3	Door (0.73×1.93)	62 kW 140 kW 340 kW 459 kW	Center elevated 0.3 m Corner elevated 0.3 m Wall elevated 0.3 m
Mowrer and Williamson (1987) [6]	No	2.44×3.66×2.44	Door (0.76×2.03)	40 kW 80 kW 160 kW	Center elevated 0.3 m Corner elevated 0.3 m Wall elevated 0.3 m
Steckler's experiment [20]	No	2.8×2.8×2.13	See Figure 5.2	31.6 kW 62.9 kW 105.3 kW 158 kW	Center at ground Corner at ground Wall at ground Center elevated 0.3 m Corner elevated 0.3 m Wall elevated 0.3 m

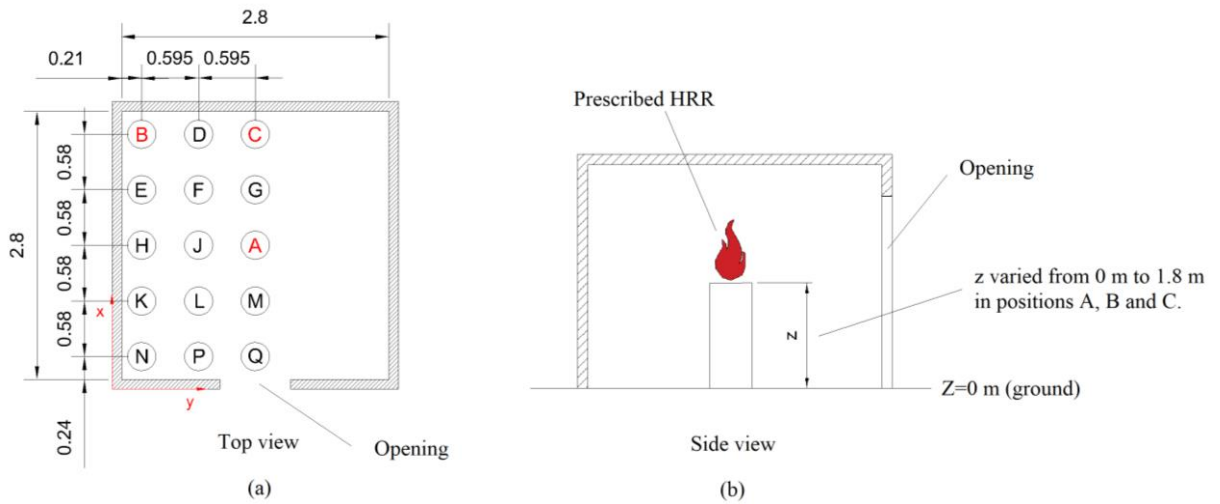


Figure 1. (a) Fire source ground positions (b) Fire source elevation

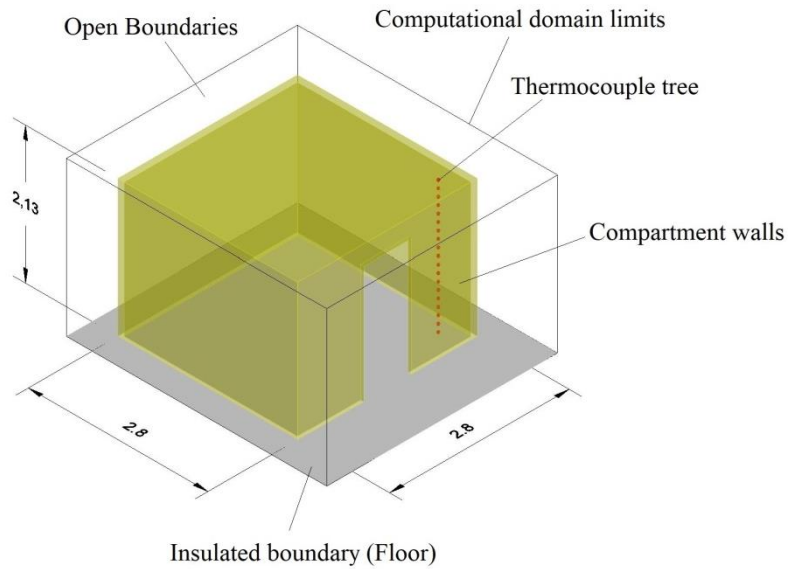


Figure 2. Room geometry and temperature measurement points

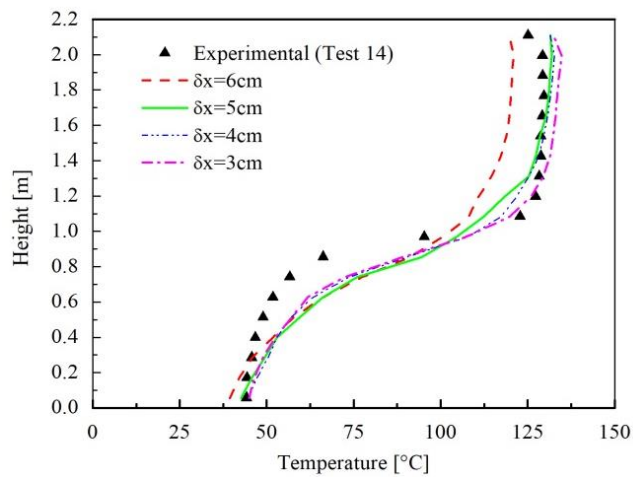


Figure 3. Mesh sensitivity analysis (Steckler's test 14).

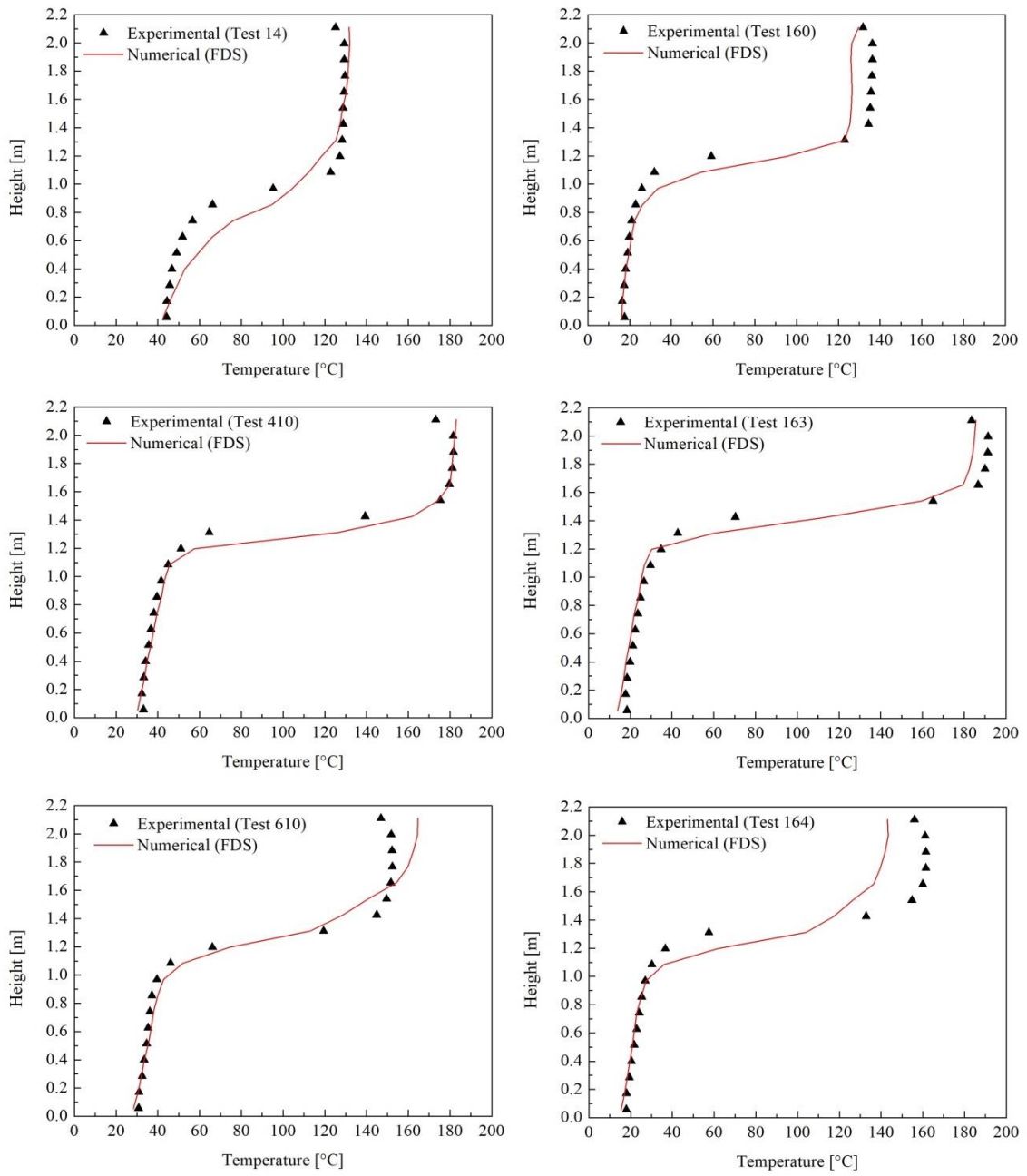


Figure 4. Temperature profiles comparison between numerical results (FDS) and experimental data (Steckler *et al.* [20]).

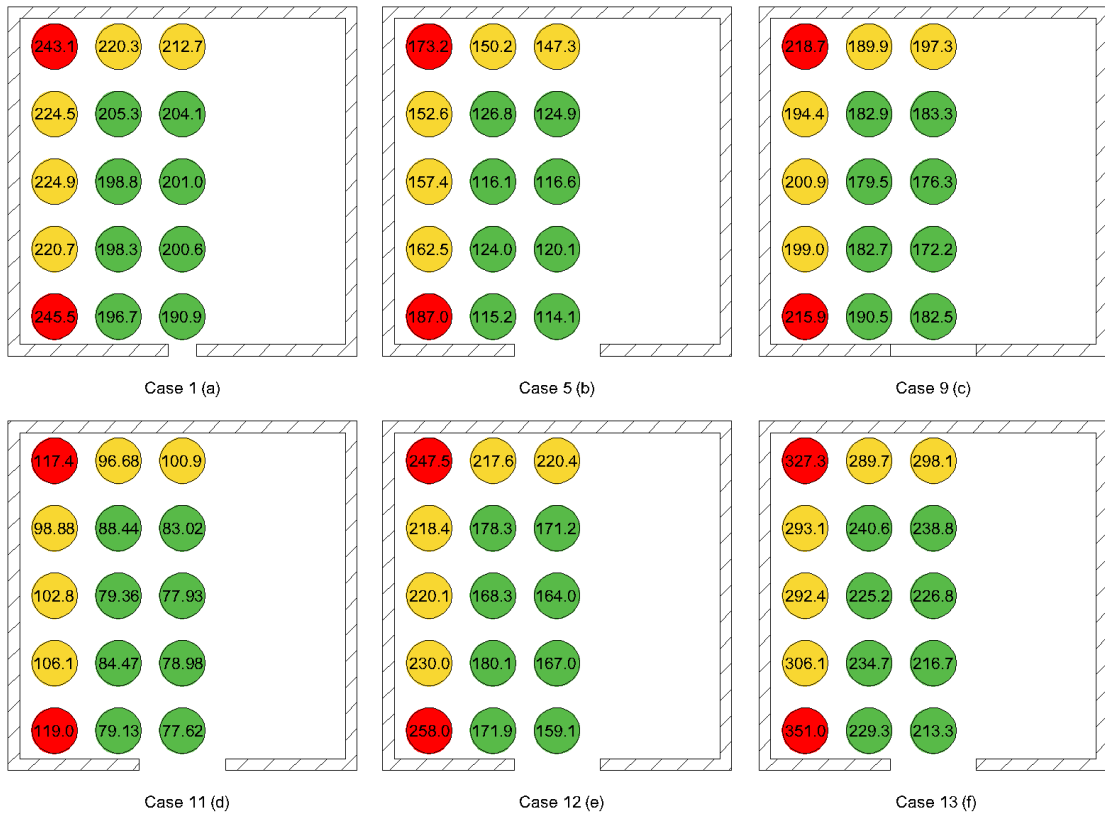


Figure 5. Average HGLT [$^{\circ}\text{C}$] in each fire source position on the ground level. Cases numeration according to Table 1 and fire positions according to Figure 1(a).

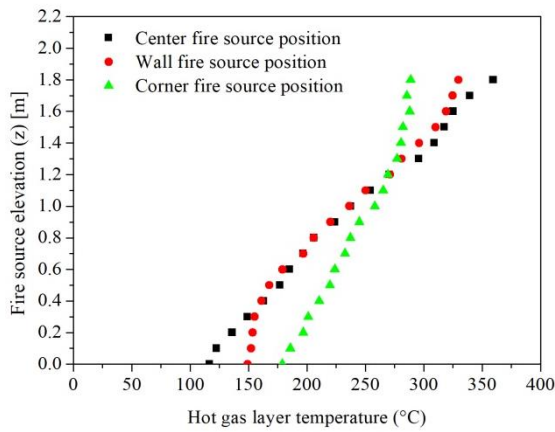


Figure 6. Relation between fire source elevation and Hot gas layer temperature

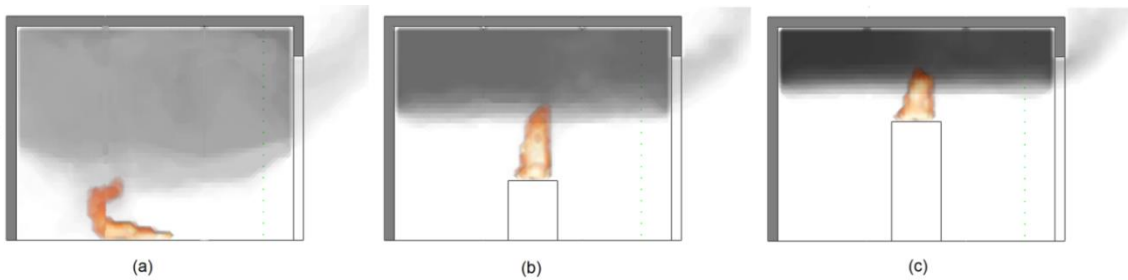


Figure 7. Illustration of the distance between the fire plume and upper gas layer for different fire source elevations: (a) $z = 0$ m, (b) $z = 0.6$ m, (c) $z = 1.2$ m.

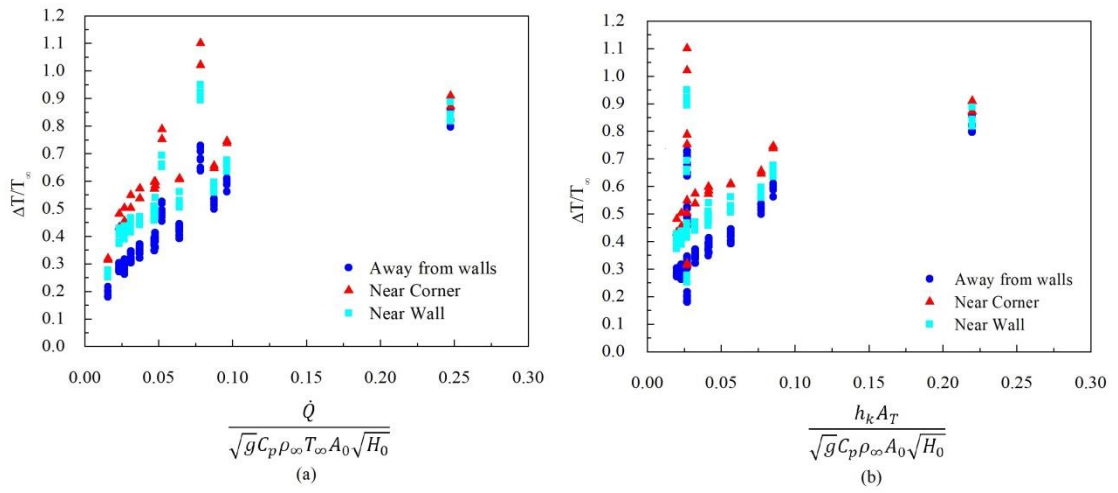


Figure 8. Dimensionless temperatures as a function of the dimensionless terms of Equation 12 (a) First term (b) second term.

1
2
3
4
5
6
7
8
9
10
11
12
13
14
15
16
17
18
19
20
21
22
23
24
25
26
27
28
29
30
31
32
33
34
35
36
37
38
39
40
41
42
43
44
45
46
47
48
49
50
51
52
53
54
55
56
57
58
59
60
61
62
63
64
65

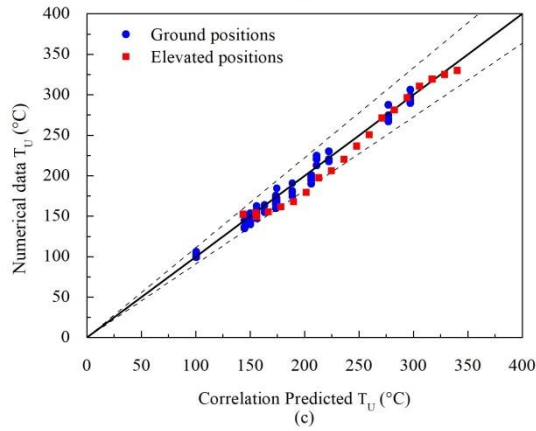
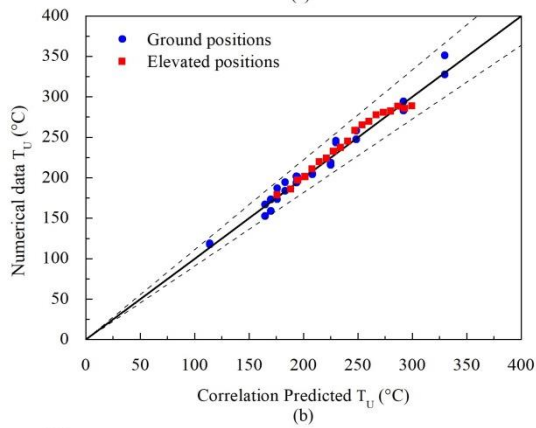
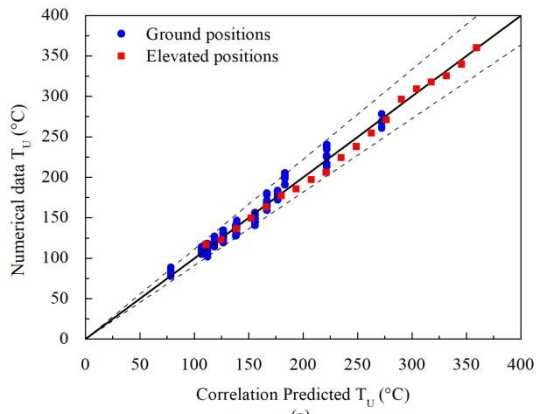
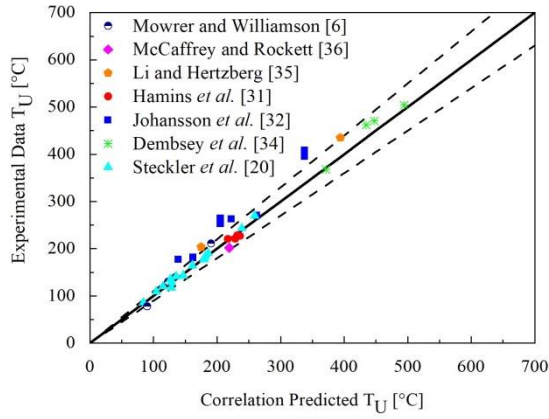
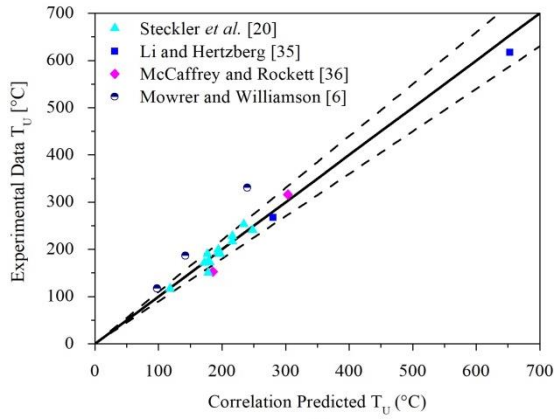


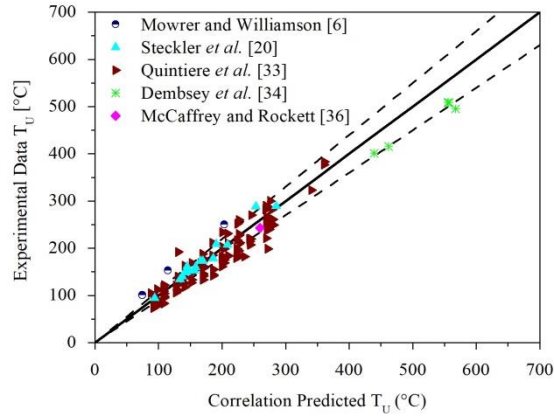
Figure 9. Comparison between upper layer temperatures predicted with Equation 14 and numerical data from FDS for fires sources (a) away from walls, (b) near a corner and (c) near a wall.



(a)



(b)



(c)

Figure 10. Comparison between HGLT predicted by the newly designed correlation and experimental data from several authors: (a) center fires, (b) near-corner fires, and (c) near-wall fires.